SERIES

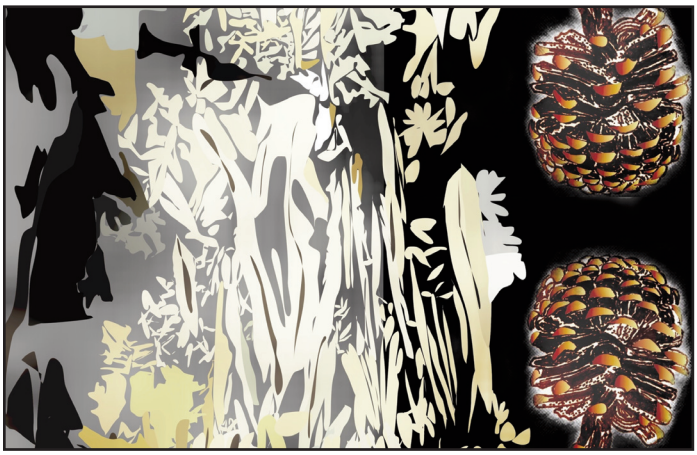

Heritage Stone 8.
Formation of Pinolitic Magnesite at Quartz Creek, British Columbia, Canada: Inferences from Preliminary Petrographic, Geochemical and Geochronological Studies

Alexandria Littlejohn-Regular, John D. Greenough and Kyle Larson

Department of Earth Environmental and Geographic Sciences
University of British Columbia Okanagan
3333 University Way, Kelowna, British Columbia
V1V 1V7, Canada
E-mail: john.greenough@ubc.ca

SUMMARY
Rocks in the Late Proterozoic Horsethief Creek Group at Quartz Creek in British Columbia display rare 'pinolitic' textures resembling those described in some sparry magnesite deposits elsewhere in the world. Elongated white magnesite crystals up to 30 cm long occur in a contrasting, dark, fine-grained matrix of dolomite, chlorite, organic material, clay minerals and pyrite. The rocks are aesthetically appealing for use in sculpture and as dimension stone. The term 'pinolite' is derived from the superficial similarities between these unusual textures and pinecones. Petrographic examination indicates that these textures formed when metasomatic fluids replaced primary sedimentary dolomite with magnesite. Fluids moved along fractures and bedding planes with repeated fracturing yielding magnesite crystals oriented in opposite directions on either side of annealed fractures, and broken magnesite crystals adjacent to later fractures. Magnesite contains dolomite microinclusions and has elevated Ca contents that are consistent with its formation by replacement of dolomite. Low concentrations of Cr, Ni, Co, Ti, Sr, and Ba in magnesite also imply formation in a metasomatic rather than a sedimentary environment. The rare earth element (REE) concentrations in the Quartz Creek magnesite are higher than those in most evaporitic magnesite and REE patterns lack the Ce and Eu anomalies that characterize carbonate rocks from sedimentary environments. Enrichment in light REE relative to heavy REE, and the similarities between dolomite, chlorite, and magnesite REE profiles, imply that metasomatic fluids modified the original sedimentary geochemical signature of the dolostones during formation of the pinolite rocks. A Late Ordovician to Early Silurian U–Pb age (433 ± 12 Ma), for titanite in the black matrix surrounding the sparry magnesite is younger than the local host rocks, and also younger than the Mesoproterozoic to Middle Cambrian stratigraphic ages of the host rocks for nearby magnesite deposits. The ca. 433 Ma titanite overlaps the ages for numerous fault-associated diatremes and volcaniclastic deposits in the area. Possibly the igneous activity furnished heat for, and/or was the source for, metasomatic fluids that produced the pinolite deposits.

RÉSUMÉ
Les roches du groupe de Horsethief Creek de la fin du Protérozoïque à Quartz Creek en Colombie-Britannique présentent des textures « pinolitiques » rares ressemblant à celles décrites dans certains dépôts de magnésite sparitique ailleurs dans le monde. Des cristaux de magnésite blancs et allongés, atteignant 30 cm de long, se trouvent dans une matrice à grains fins, sombre et contrastante, et composée de dolomie, de chlorite, de matière organique, de minéraux argileux et de pyrite. Les roches sont esthétiquement attrayantes pour un usage en sculpture et en tant que pierre de taille. Le terme « pinolite » est dérivé des similitudes superficielles entre ces textures inhabituelles et les pommes de pin. L'examen pétrographique indique que ces textures se sont formées lorsque les fluides métasomatiques ont remplacé la dolomie sédimentaire pri-

Geoscience Canada, v. 48, https://doi.org/10.12789/geocanj.2021.48.177 pages 117–132

GC Data Repository: Heritage Stone Series at https://GAC.ca/GC-data-repository

maire par de la magnésite. Les fluides se sont déplacés le long des fractures et des plans de stratification présentant des fracturations répétées, produisant des cristaux de magnésite orientés dans des directions opposées de chaque côté des fractures recuites, et des cristaux de magnésite brisés adjacents aux fractures ultérieures. La magnésite contient des micro-inclusions de dolomie et a des teneurs élevées en Ca qui sont compatibles avec sa formation par remplacement de la dolomie. De faibles concentrations de Cr, Ni, Co, Ti, Sr et Ba dans la magnésite impliquent également la formation dans un environnement métasomatique plutôt que sédimentaire. Les concentrations d'éléments des terres rares (ETR) dans la magnésite de Quartz Creek sont plus élevées que celles de la plupart des magnésites évaporitiques et les profils d'ETR ne présentent pas les anomalies en Ce et Eu qui caractérisent les roches carbonatées des environnements sédimentaires. L'enrichissement en ETR légers par rapport aux ETR lourds, et les similitudes entre les profils des ETR de la dolomie, de la chlorite et de la magnésite, impliquent que les fluides métasomatiques ont modifié la signature géochimique sédimentaire originale des dolomies lors de la formation des pinolites. Un âge U–Pb de la fin de l'Ordovicien au début du Silurien (433 ± 12 Ma), pour la titanite dans la matrice noire entourant la magnésite sparitique, est plus récent que celui des roches hôtes locales, et également plus récent que les âges stratigraphiques du Mésoprotérozoïque au Cambrien moyen des roches hôtes des dépôts de magnésite voisins. La titanite d'environ 433 Ma chevauche les âges de nombreux diatrèmes et dépôts volcanoclastiques associés à des failles dans la région. Il est possible que l'activité ignée a fourni la chaleur et/ou a été la source des fluides métasomatiques qui ont produit les dépôts de pinolites.

Traduit par la Traductrice

INTRODUCTION

Rocks exhibiting spectacular pinolitic textures were discovered in 2018 by placer gold miners working at Quartz Creek in the Northern Purcell Mountains, near Golden in southeastern British Columbia (Fig. 1). The term 'pinolite' has been used for rare, aesthetically pleasing textures resembling pinecones. These textures are found in sparry magnesite deposits that are generally hosted in metamorphosed Proterozoic and Paleozoic sedimentary rocks (Pohl 1989; Pohl 2011, p. 336). Sparry magnesite deposits are also informally referred to as Veitsch-type magnesite deposits in reference to a former mine in Austria, where magnesite forms stratiform lenses within marine platform sedimentary rocks (Redlich 1909). Pinolitic textures found in parts of these deposits typically consist of elongated white magnesite crystals in a fine-grained dark matrix consisting of chlorite, organic material, pyrite, talc and dolomite (Pohl 2011, p. 336). These textures have also been described from Russia, Spain and elsewhere in Canada, primarily in operating magnesite mines (Simandl and Hancock 1991; Lugli et al. 2000; Krupenin and Ellmies 2001; Krupenin 2005; Kilias et al. 2006; Azim Zadeh et al. 2015; Paradis and Simandl 2018).

The pinolite rocks at Quartz Creek are hosted by Neoproterozoic carbonate rocks of the Horsethief Creek Group (Fig. 1). Pinolitic textures have also been reported at Mount Brussilof Mine, a magnesite deposit located approximately 130 kilometres southeast of the study area (Fig. 1 inset). At Mount Brussilof, they are interpreted as diagenetic or metasomatic replacement textures (Simandl and Hancock 1991; Paradis and Simandl 2018). Other significant sparry magnesite occurrences in southeastern British Columbia include the Marysville, Brisco and Driftwood Creek deposits (Fig. 1; Hancock and Simandl 1992; Simandl and Hancock 1992, 1999). However, these do not necessarily contain widely developed pinolite textures.

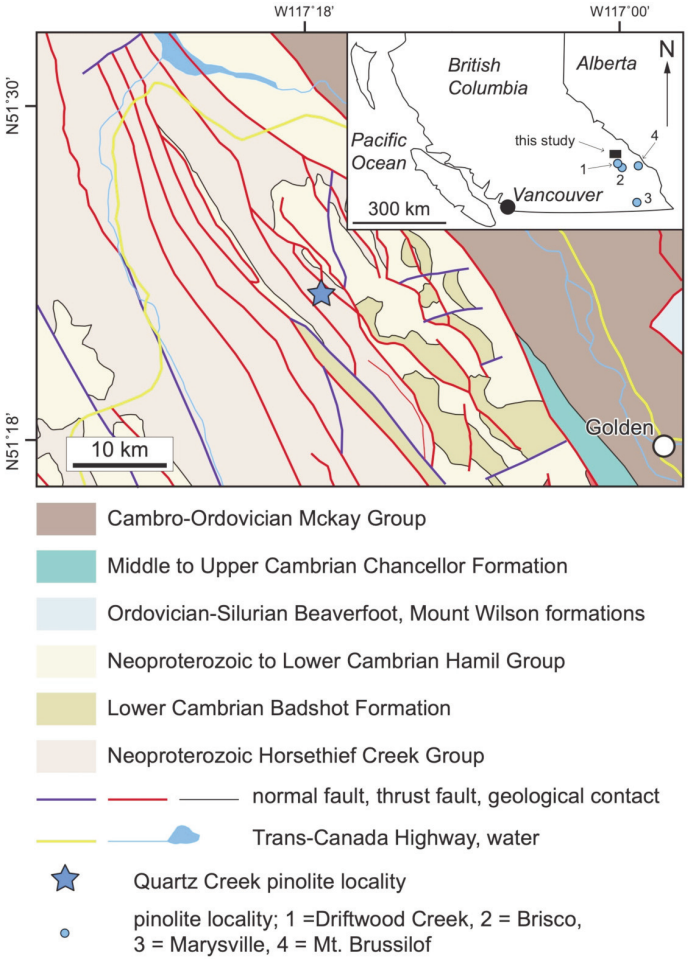

Figure 1. Geological map of the area surrounding the Quartz Creek pinolite quarry. Quarry location and the sampling site are shown. The index map shows location of the study area and selected magnesite deposits in southeastern British Columbia. Map redrafted using geological data from MapPlace [https://www2.gov.bc.ca/gov/content/industry/mineral-exploration-mining/british-columbia-geological-survey/mapplace].

The genesis of sparry magnesite deposits and pinolite has been debated at length, and the two principal hypotheses propose syngenetic and epigenetic origins, respectively (e.g. Simandl and Hancock 1999; Marshall et al. 2004). Studies in support of a syngenetic origin suggest that magnesite was deposited under evaporitic conditions or during diagenetic recrystallization of a magnesite protolith deposited as a chemical precipitate in marine or lacustrine settings (Pohl 1990). In contrast, the epigenetic hypothesis invokes hydrothermal metasomatic replacement of dolomitized, permeable carbon-

ates by magnesite. Metasomatic hydrothermal models involving Mg-rich fluids have been suggested for sparry magnesite deposits in Spain and Austria (Pohl and Siegl 1986; Nesbitt and Prochaska 1998; Kilias et al. 2006; Azim Zadeh et al. 2015) as well as in Canada (Simandl and Hancock 1991, 1992, 1999; Hancock and Simandl 1992; Simandl et al. 1992). This paper represents a contribution to the debate surrounding the origins of such textures.

The Quartz Creek pinolite rocks discussed here are of economic interest. Their exceptional and aesthetically pleasing textures (Fig. 2) make them valuable for carving and dimension stone and led to the establishment of the first pinolite quarry in North America. The Quartz Creek site is also of interest in the context of the debate concerning the origin(s) of pinolite textures and associated magnesite deposits. The research summarized in this paper was completed as part of a thesis project by the senior author, focused on optical and scanning electron microscopy and major and trace element analysis of whole-rock samples and constituent minerals. Electron microprobe (EMPA) analysis and laser ablation inductively coupled plasma mass spectrometry (LA-ICP-MS) trace element analysis were used to determine mineral compositions. We also report a U–Pb titanite age, obtained using LA-ICP-MS methods, that probably pinpoints the timing of pinolite formation. The study compares the data from Quartz Creek with results for other sparry magnesite deposits including local deposits which exhibit similar pinolite textures (Simandl and Hancock 1991). Our research is limited to a small number of analyses and a single U–Pb age; more work is required to substantiate and extend its findings. Nevertheless, the results are interesting, and provide new information about an unusual semi-precious stone that may have wider importance in British Columbia. Although the Quartz Creek pinolite quarry is not associated with a sparry magnesite deposit exploited for magnesium, understanding its origins may provide useful insight into the genesis of such deposits.

GEOLOGICAL SETTING AND SAMPLE COLLECTION

Based on geological mapping by Poulton and Simony (1980), the Quartz Creek pinolite quarry is hosted in the Neoproterozoic Horsethief Creek Group but its precise stratigraphic position within the group is unclear. The following summary of regional geology applies to Figure 1 and the surrounding area.

The Quartz Creek pinolite rocks occur in the Dogtooth Range, the most northern subrange of the Purcell Mountains, and within the Horsethief Creek Group, which is in turn a subdivision of the Neoproterozoic Windermere Supergroup. The regional geology was documented by Wheeler and Fox (1962) and Kubli (1990) and the stratigraphy and sedimentology of the Horsethief Creek Group was studied by Poulton (1973) with most emphasis on the upper unit of carbonate rocks. The Dogtooth Range appears to have a relatively simple deformation history consisting of a single, extended phase of northeastward-directed compression under low grade, greenschist facies metamorphism (Kubli 1990). The rocks of the Horsethief Creek Group are cut by several north-easterly-directed thrust faults (Poulton 1973), and the pinolite locality sits within a structural subdivision termed the Quartz Creek thrust sheet (Fig. 1). The term 'slate' is commonly used for argillitic rocks interpreted to be derived from shales, and the term 'grit' is used for coarse sandstones to fine pebble conglomerates (Poulton and Simony 1980).

Available mapping does not distinguish formal units within the Horsethief Creek Group but its overall stratigraphy is known in general terms (Kubli 1990). These sedimentary rocks transition upward over ~3000 m from beds dominated by slates (Basal Pelite), coarse sandstones and slate (Lower Grit), into a carbonate-bearing unit (Baird Brook unit, up to 140 m thick), followed by another siliciclastic unit (Upper Grit), a slate unit (Slate Division) and a thick limestone and dolostone unit (Carbonate Division, up to 390 m thick). The top of the Horsethief Creek Group section is defined by another siliciclastic unit up to 230 m thick (Kubli 1990). The stratigraphic position of the carbonate rocks that host the pinolite at Quartz Creek is uncertain; they could be part of the Baird Brook unit or the upper Carbonate Division. The Baird Brook unit is dominated by slate and limestone interpreted to have formed during sea-level rise associated with a reduction in the supply of coarse clastic detritus (Kubli 1990). There is no previous record of magnesite or pinolitic textures in the area, but a massive dolostone unit in the Carbonate Division was documented by Poulton and Simony (1980). The only clear stratigraphic or structural constraint on the timing of pinolite texture formation is given by the Neoproterozoic age of the Horsethief Creek Group, which provides an upper limit.

Rocks that display well-developed pinolitic textured rocks form weathered outcrops, and occur as relatively unweathered boulders, in steep scree slopes on the east side of Quartz Creek approximately 25 km northwest of Golden (Fig. 1). Numerous specimens were collected from the quarry site, which is located at 117°16'42.25" W and 51°23'7.43" N. Five samples, representing end-member variations in texture, were selected for detailed study. Specimens PIN 1 and 2 are from outcrop at the quarry site whereas PIN 3, 4 and 5 are locally derived boulders showing textures that are not represented in the more limited outcrop at the site.

ANALYTICAL METHODS

Full details of analytical procedures are given in Appendix A (see Geoscience Canada data repository). Polished thin sections were examined using a petrographic microscope, mineral identifications were confirmed by SEM EDS (Scanning Electron Microscope, Energy Dispersive Spectrometry) and analyses and textures were documented with back-scattered electron (BSE) images. The whole-rock samples were analyzed for major and trace elements at ACME Analytical Laboratories, Vancouver, by ICP-ES (Inductively Coupled Plasma - Emission Spectroscopy) and ICP-MS (Mass Spectrometry), respectively. All SEM work and all mineral analyses were performed at the Fipke Laboratory for Trace Element Research (FiLTER) of the University of British Columbia, Okanagan campus. Major element mineral analyses were performed by Electron

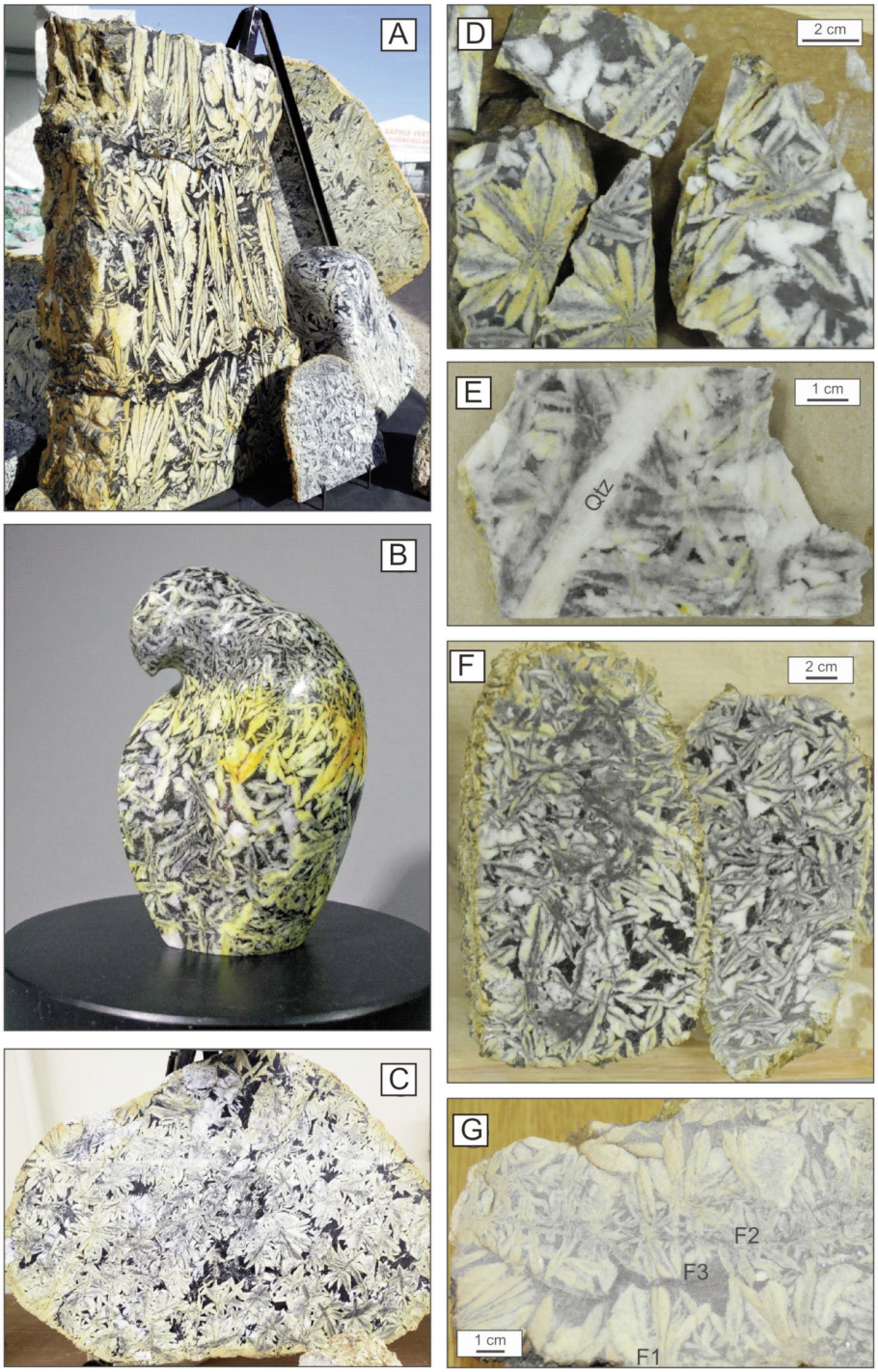

Figure 2. Photographs of pinolite from Canadian Pinolite's Quartz Creek quarry. A) large dimension-stone slab ~120 cm tall, exhibiting light-colored magnesite crystals up to ~ 30 cm long radiating toward the centre of the slab from two irregular, subhorizontal fractures in the upper and lower third of the rock. Black material in the fractures, and between magnesite crystals is interpreted as relict host rock. Photograph courtesy of Ian Burak. B) Bird sculpture (~ 35 cm tall) carved from pinolite. Yellow areas reflect oxidation due to incipient weathering. Sculpture and photograph by Deborah Wilson (Vernon, BC); photograph from Ian Burak who owns the image and the sculpture. C) Photograph showing a ~ 50 cm-wide dimension-stone slice through a pinolite rock with typical, radiating, sparry magnesite crystals surrounded by darker matrix rock. D) Assorted slices through sample PIN 1 showing magnesite with a radiating texture. The photograph also shows the colour contrast between magnesite crystals and dark matrix material. Together, the radiating texture and colour contrast create an unusual, aesthetically-pleasing rock that is in demand from sculptors and for dimension stone. E) Close-up photograph of a slice through sample PIN 2 showing a quartz vein cutting the rock. F) Pinolite sample PIN 5 showing pinolite texture. Magnesite grains are separated by a thin dark matrix. G) Pinolite sample PIN 4 showing magnesite crystals growing up (in the photograph) from a fracture (F1) along which the sample was broken in freeing it from the outcrop. In the centre of the rock and fracture system there is a faint line (F2) where crystals apparently grew both up and down and away from the poorly-defined fracture. The rock underwent another episode of fracturing (F3) that terminates crystals previously grown from F1 and F2, but the dark country rock forming the matrix in this fracture shows no preferential tendency to break at the matrix-magnesite boundaries, suggesting annealing after F3. Many of the magnesite crystals have a feather-like appearance with a line of dark inclusions parallel to the long axes of the crystals. Faint orange coloration reflects minor, incipient weathering at the outcrop surface.

Microprobe Analysis (EMPA) and mineral trace element analyses by laser-ablation (LA-ICP-MS). The U–Pb dating of titanite in sample PIN 4 used *in-situ* LA-ICP-MS.

RESULTS

Petrography and Mineralogy

Specimens PIN 1 to 5 were selected for detailed petrographic and geochemical analysis because they represent the wide range of textures present at Quartz Creek, and all exhibit typical pinolitic textures where large light-coloured crystals of magnesite occur in a dark matrix (Fig. 2). These magnesite crystals are elongate (prismatic or scalenohedral; length/width ratios of 2 to 4), typically exhibit a black band of inclusions parallel to their long axes and are generally separated from one another by thin (mm – cm) irregular patches of dark matrix. The large magnesite crystals are the dominant component of all samples examined in detail, as illustrated in Figure 2. The maximum size of magnesite crystals (long dimension) varies from about 1 cm in sample PIN 3 to 4.4 cm in sample PIN 1. All samples, excluding PIN 3, are illustrated in Figure 2 (see panels D, F and G). Locally, magnesite crystals reach lengths of 30 cm, as shown in a large display sample (Fig. 2A). Crystal sizes can also vary over short distances, as shown in the bird sculpture (Fig. 2B). Specimen PIN 1 (Fig. 2D) contains radiating rosettes of magnesite crystals but in others the crystals appear to be randomly oriented (Fig. 2F). Specimen PIN 2 contains a quartz vein ~ 1 cm wide, cutting through magnesite crystals (Fig. 2E). Some magnesite crystals appear to have nucleated on the walls of fractures and to have grown away from the fracture centre. The fractures and fracture systems are cm to tens of cm wide and underwent multiple episodes of brittle opening that broke apart the earliest-formed magnesite crystals (Fig. 2A, 2G). Black relict wall rock forms the dark material in fractures and wraps around the magnesite crystals but remains strongly adhered to them, making the material coherent for cutting and polishing. Weathering close to exposed rock surfaces produces yellow to orange and locally brown discolouration, as shown by several samples illustrated in Figure 2.

Back-scattered electron microscope images (Fig. 3) reveal that dolomite is more abundant than originally estimated from macroscopic examination. Dolomite forms cm-sized idiomorphic crystals associated with anhedral sparry magnesite (Fig. 3A) but also occurs as microinclusions (≤ 10 μm to 200 μm) within magnesite (Fig. 3B) and as larger multigrain masses included in magnesite (Fig. 3C). The dark matrix consists of

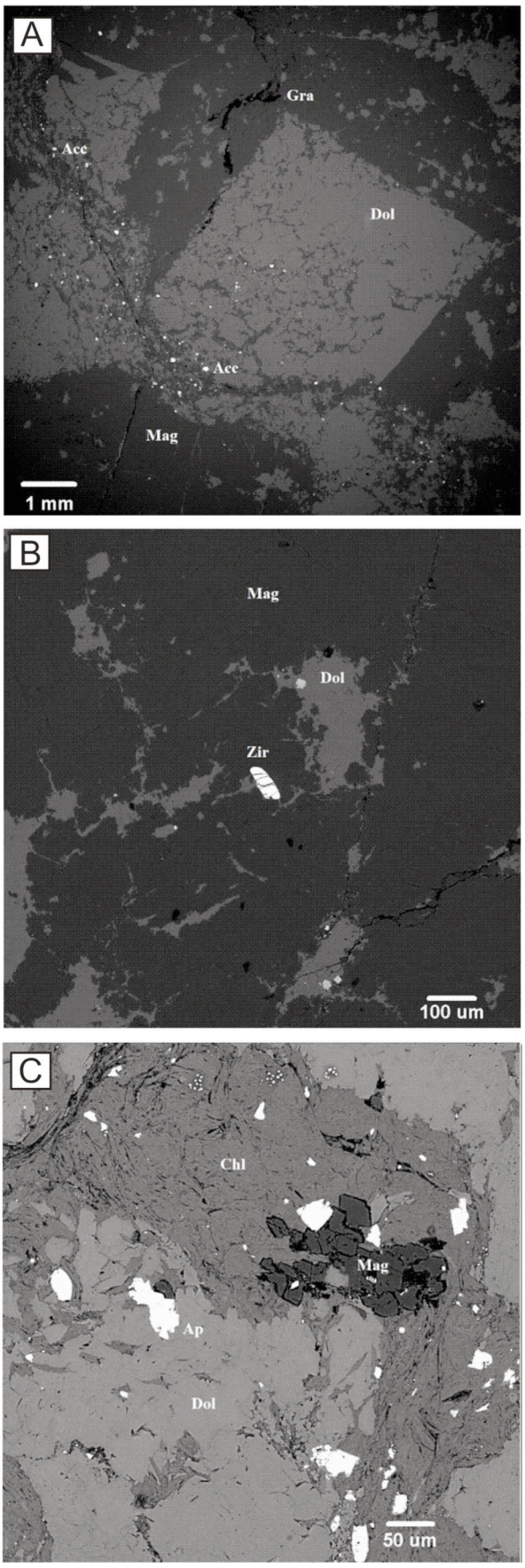

Figure 3. *(opposite)* Back-scattered electron (BSE) images showing dolomite (Dol; light grey), magnesite (Mag; dark grey) and chlorite (Chl). A, B) Images from sample PIN 4 in which accessory minerals including zircon, apatite, titanite, rutile and Fe-Ti oxides are bright white (labelled Acc) and small black patches and irregular lines are graphite (Gra). Relict dolomite patches and microinclusions occur in the magnesite, and idiomorphic (recrystallized?) dolomite is locally riddled with magnesite. A rounded (detrital?) 50 μm zircon occurs in the centre of image B. C) Back-scattered electron (BSE) image of sample PIN 5 showing chlorite (Chl) within dolomite (Dol). A magnesite (Mag) grain and apatite crystals (white grains) occur within chlorite and a large apatite grain (Ap) occurs in dolomite.

https://doi.org/10.12789/geocanj.2021.48.177

fine-grained dolomite, minor magnesite (< 10%), Mg-chlorite (< 10%), calcite, quartz, and several other accessory minerals (Fig. 3A). The Mg-chlorite was identified as clinochlore, and locally forms sinuous masses bearing various accessory minerals, idiomorphic magnesite inclusions and elongate carbonaceous inclusions oriented parallel to cleavage (Fig. 3C). The carbonaceous material also forms ≤ 0.2 mm wide stringers that wrap around magnesite and dolomite grains and also occur within grains (Fig. 3A). The carbonaceous material most likely consists of graphite considering the regional greenschist facies metamorphism reported by Kubli (1990). Non-carbonate accessory minerals make up ≤ 10% of the samples and include rutile, apatite, pyrite, zircon, titanite, micas (paragonite and muscovite), iron oxides and clay minerals. Rounded to irregular, small (≤ 60 μm) fluorapatite grains are scattered within magnesite, chlorite, and dolomite grains (Fig. 3C). These accessory minerals, including the titanite used for dating, are most abundant in the black matrix material, between larger magnesite and dolomite crystals and are typically concentrated in narrow bands that have a thin (≤ 1 mm) linear array of magnesite grains in the centre (Fig. 3A). Zircon grains in the matrix show variable sizes (30 μm – 100 μm), are very diverse in shape (angular to well-rounded) and exhibit varied internal textures (Fig. 3B).

Whole Rock and Mineral Geochemistry

Whole rock major and trace element contents of the pinolite specimens are highly variable (Table 1; Fig. 4). For example, MgO varies from 18.2 to 37.8 wt. % and Sr varies from 27 to 180 ppm. MgO shows a negative correlation with CaO and Sr, and a positive correlation with Fe_2O_3, but has no clear relationship with SiO_2, Al_2O_3 or trace elements (e.g. Zr and Y). The interpretation of geochemical patterns is hampered by the small number of samples that were analyzed and a larger dataset might reveal more coherent patterns.

Analyses of the dominant minerals (Table 2) show that chlorite and magnesite have the highest FeO contents, as would be expected. The high CaO and Sr contents of dolomite are also predictable, but this mineral also seems to have high Y and REE compared to magnesite and chlorite (Table 2). Enrichment in High Field Strength Elements (HFSE: Zr, Hf, U, Th) is seen in chlorite. A primitive-mantle-normalized spider diagram for whole rock analyses (Fig. 5A) displays strong negative Ti anomalies and positive Th and U anomalies. These profiles are compared to those of average shale, which shows higher normalized concentrations for most elements (Fig. 5A). The normalized profiles for the Quartz Creek samples are somewhat more jagged than those of average shale, with prominent positive Th, U, Sr, Sm and Eu anomalies and negative Ba, Nb, K, Zr, Hf and Ti anomalies (Fig. 5A). A similar primitive-mantle-normalized spider diagram for average mineral analyses (Fig. 5B; average of data in Table 2) shows that chlorite is depleted in most elements, but has positive Zr, Hf, Sr and U anomalies. Dolomite shows negative Ba and positive Eu, Sm and Sr anomalies. Note that both magnesite and dolomite have Ti concentrations below the detection limit, so values for this element cannot be represented. The trace element pattern for magnesite resembles that for dolomite in most respects, but magnesite tends to have lower normalized concentrations for most of the analyzed elements.

Table 1. Whole rock major and trace element compositions of pinolite samples.

Element	PIN 1	PIN 2	PIN 3	PIN 4	PIN 5	DL
SiO_2	4.55	14.52	3.30	8.68	9.39	0.01
TiO_2	0.03	0.01	0.02	0.06	0.02	0.01
Al_2O_3	0.96	0.28	0.51	1.16	0.29	0.01
Fe_2O_3	0.93	0.88	1.39	1.96	0.77	0.01
MnO	0.02	0.02	0.03	0.03	0.02	0.01
MgO	21.23	18.23	30.79	37.77	20.23	0.01
CaO	26.56	24.97	16.05	3.39	25.65	0.01
Na_2O	0.12	0.03	<DL	0.15	<DL	0.01
K_2O	0.06	0.03	<DL	0.09	0.01	0.01
P_2O_5	0.03	<DL	0.03	0.03	0.02	0.01
LOI	45.10	40.70	47.40	46.10	43.30	
Sum	99.59	99.67	99.52	99.40	99.70	
Tot C	12.76	11.59	6.80	12.96	11.90	0.02
Rb	2.80	1.20	<DL	3.35	<DL	0.10
Cs	0.10	<DL	<DL	0.20	<DL	0.10
Sr	103	166	90.0	26.6	181	0.50
Ba	4.00	4.00	4.00	5.50	3.00	1.00
Zr	10.5	19.9	5.30	69.6	12.5	0.10
Hf	0.30	0.50	0.20	1.75	0.30	0.10
Nb	0.90	1.10	0.70	2.20	0.20	0.10
Th	0.70	0.60	0.50	2.25	0.70	0.20
U	0.80	0.20	0.50	0.65	0.40	0.10
La	3.60	2.20	1.50	2.00	2.90	0.10
Ce	5.80	5.20	3.90	4.25	6.30	0.10
Pr	0.89	0.83	0.73	0.83	1.00	0.02
Nd	5.10	5.20	4.40	5.80	5.30	0.30
Sm	2.63	3.87	1.04	3.38	1.64	0.05
Eu	0.91	1.27	0.45	1.07	0.59	0.02
Gd	2.39	5.07	0.98	3.24	1.38	0.05
Tb	0.24	0.64	0.18	0.33	0.16	0.01
Dy	0.87	2.71	0.49	1.37	0.71	0.05
Ho	0.15	0.45	0.14	0.22	0.13	0.02
Er	0.34	0.91	0.22	0.53	0.37	0.03
Tm	0.04	0.10	0.09	0.07	0.05	0.01
Yb	0.26	0.57	0.18	0.45	0.25	0.05
Lu	0.04	0.07	0.07	0.07	0.04	0.01
Y	4.70	13.00	4.40	6.70	4.30	0.10
Ga	0.70	<DL	<DL	0.70	<DL	0.50
Ni	2.60	0.80	1.70	3.40	0.40	0.10
Co	3.70	0.30	2.30	2.20	<DL	0.20
Cu	3.50	0.80	2.85	1.30	1.20	0.10
Pb	1.70	0.60	0.80	0.90	0.20	0.10
As	2.70	<DL	1.40	4.50	<DL	0.50
W	40.4	1.80	0.70	3.00	1.00	0.50
Sb	0.20	<DL	0.20	<DL	<DL	0.10

Notes: Major element oxides in wt. %. Total Fe as Fe_2O_3.
Sum = Sum of oxides + LOI (Loss on Ignition).
Tot C = Total carbon in Wt. %. Trace elements in ppm.
DL= Detection Limit; <DL indicates results below Detection Limits.
PIN4 = average of 2 replicate analyses for most elements.
PIN5 = average of 2 replicate analyses for Cu, Pb, Ni, As, Sb.
For details of accuracy and precision, see analytical methods.

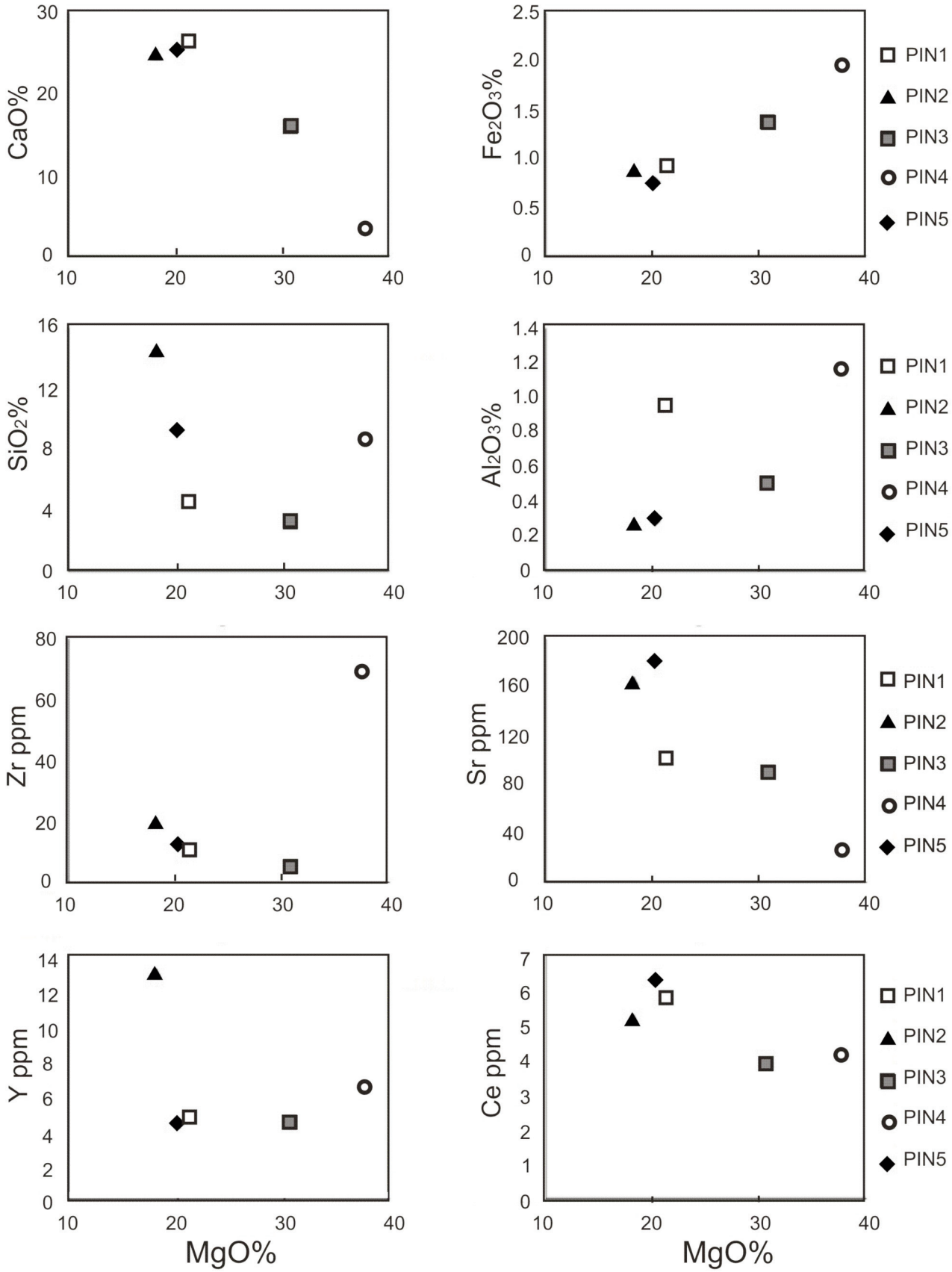

Figure 4. Relationship between MgO wt. % and major element oxides and trace elements for whole rock analyses of Quartz Creek Pinolite rocks.

https://doi.org/10.12789/geocanj.2021.48.177

Table 2. Mineral compositions for magnesite, dolomite and chlorite, determined by electron microprobe as major element oxides (wt.%) and by LA ICP-MS as trace elements (ppm).

Analysis Specimen	M-1 PIN 3	M-2 PIN 3	M-3 PIN 3	D-1 PIN 3	D-2 PIN 3	D-3 PIN 3	C-1 PIN 5	C-2 PIN 5	C-3 PIN 5	DL
SiO_2	<DL	0.01	<DL	<DL	<DL	<DL	30.49	30.6	30.28	0.01
TiO_2	<DL	<DL	<DL	<DL	<DL	<DL	0.02	0.02	0.01	0.01
Al_2O_3	<DL	<DL	<DL	<DL	<DL	<DL	21.33	20.5	20.92	0.01
FeO	1.48	2.51	1.40	0.49	0.58	0.51	1.60	1.92	1.54	0.01
MnO	<DL	0.05	0.03	0.03	0.03	0.01	<DL	0.01	0.01	0.01
MgO	48.46	50.5	49.17	24.3	24.7	25.63	35.15	34.65	32.28	0.01
CaO	0.86	0.10	0.71	32.64	33.63	33.73	0.02	0.03	0.05	0.01
Na_2O	0.01	0.02	0.02	0.02	<DL	<DL	0.06	0.05	0.07	0.01
K_2O	<DL	0.01	<DL	<DL	<DL	<DL	0.08	0.04	0.05	0.01
P_2O_5	<DL	<DL	<DL	0.03	0.03	0.01	0.03	0.03	0.05	0.01
F	<DL	<DL	<DL	<DL	<DL	<DL	0.70	0.74	0.76	0.01
Cl	<DL	<DL	<DL	<DL	<DL	<DL	0.03	0.07	0.11	0.01
Total	50.81	53.19	51.34	57.5	58.97	59.89	89.50	88.63	86.13	
Sc	1.09	0.53	0.66	1.74	1.03	0.29	0.27	0.52	1.55	0.18
V	4.03	3.48	4.05	5.74	4.21	1.6	47.4	51.8	78.7	0.05
Cr	<DL	<DL	<DL	<DL	<DL	<DL	67.2	87.7	77.7	1.71
Co	1.82	0.04	0.04	0.2	<DL	<DL	0.66	1.71	2.77	0.03
Ni	1.20	<DL	<DL	<DL	<DL	<DL	24.3	28.6	32.8	0.97
Cu	1.07	<DL	<DL	<DL	<DL	<DL	28.5	2.02	5.32	0.50
Zn	3.66	2.36	3.62	2.26	2.02	1.41	12.3	9.89	13.7	1.24
As	1.49	<DL	<DL	1.30	<DL	<DL	2.16	2.59	17.3	0.88
Rb	0.64	<DL	<DL	0.17	<DL	<DL	0.27	0.14	0.65	0.05
Sr	19.2	1.43	2.67	143	153	89.7	13.8	9.11	123	0.05
Y	3.75	3.87	4.37	19.4	17.4	2.82	2.20	2.44	7.67	0.02
Zr	4.26	1.28	0.20	0.22	<DL	<DL	38.9	119	169	0.03
Nb	0.32	<DL	<DL	0.19	<DL	<DL	5.75	0.61	5.05	0.01
Sb	0.45	<DL	<DL	0.27	<DL	<DL	<DL	0.43	4.43	0.13
Ba	1.55	0.20	0.68	0.35	0.19	0.01	1.72	20.2	36.9	1.09
La	0.86	0.62	0.77	5.11	4.65	0.50	0.52	0.22	0.62	0.04
Ce	3.66	3.59	4.2	18.2	16.7	1.94	2.26	1.1	1.46	0.05
Pr	0.94	0.73	0.8	3.5	3.06	0.37	0.36	0.13	0.27	0.04
Nd	4.00	4.71	5.13	20.8	19.0	2.50	2.35	0.92	1.73	0.50
Sm	1.83	1.52	1.67	9.29	8.65	1.25	0.95	0.40	0.75	0.07
Eu	0.92	0.69	0.72	3.61	2.85	0.40	0.27	0.11	0.21	0.03
Gd	1.27	1.19	1.06	8.96	7.72	1.20	0.78	0.43	0.59	0.04
Tb	0.38	0.09	0.10	1.03	0.71	0.11	0.06	0.03		0.03
Dy	0.83	0.53	0.55	3.74	3.20	0.60	0.37	0.39	0.89	0.03
Ho	0.44	0.09	0.11	0.79	0.55	0.09	0.09	0.06	0.19	0.03
Er	0.61	0.31	0.36	1.63	1.22	0.19	0.21	0.3	0.87	0.03
Tm	0.35	<DL	0.03	0.36	0.15	0.03	0.02	0.03	0.14	0.02
Yb	0.55	0.25	0.26	1.15	0.90	0.13	0.18	0.34	0.91	0.04
Lu	0.34	<DL	<DL	0.31	0.12	<DL	0.03	0.04	0.12	0.02
Hf	0.39	<DL	<DL	0.18	<DL	<DL	0.89	3.24	4.49	0.03
Ta	0.32	<DL	<DL	0.19	<DL	<DL	0.37	0.02	0.18	0.03
Pb	0.58	<DL	<DL	0.28	<DL	<DL	0.21	1.02	3.14	0.11
Th	0.53	0.06	0.06	0.35	0.10	0.03	2.83	6.48	6.94	0.01
U	0.70	0.08	0.03	0.26	<DL	<DL	3.45	5.78	7.29	0.01

Notes: Major element concentrations in oxide wt. % with all Fe as FeO. Trace elements in ppm.
EMPA = electron microprobe analysis; DL = Average detection limit. < DL is below Detection Limit.
For details of precision and accuracy, see analytical methods.

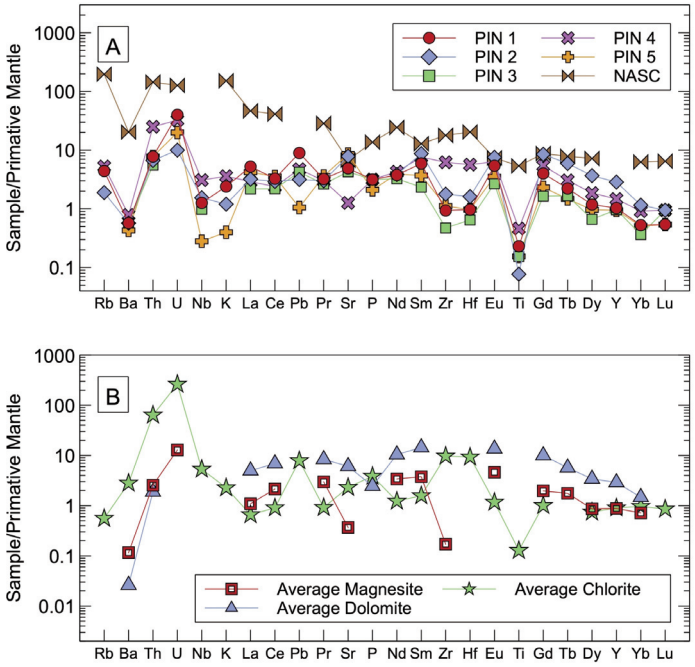

Figure 5. Primitive-mantle-normalized spider diagrams. A) Whole rock analyses (data in Table 1) and North America Shale Composite (NASC) from Gromet et al. (1984). B) average mineral analyses by LA ICP-MS (data in Table 2). Elements missing in part B patterns were below detection limit in one or more of the analyses and are not included. Primitive mantle normalizing values are from McDonough and Sun (1995).

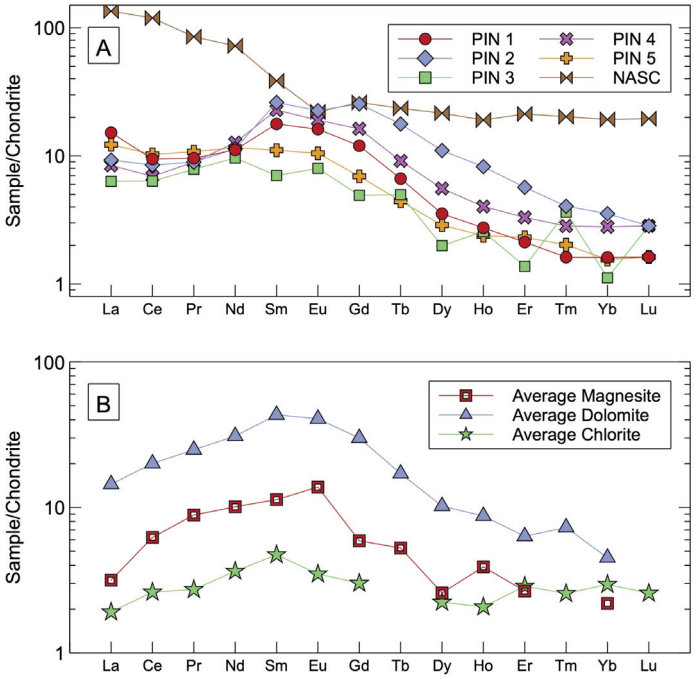

Figure 6. A) Chondrite-normalized REE patterns for whole rock pinolite analyses (Table 1) and North American Shale Composite (Gromet et al. 1984). B) Chondrite normalized REE patterns for averages of LA-ICP-MS mineral analyses in Table 2. Missing points reflect that one or more analyses were below the detection limit and the average not plotted. Chondrite normalizing values from McDonough and Sun (1995).

Rare Earth Elements

Rare Earth Element (REE) concentrations from whole rock and mineral analyses are listed in Table 1 and Table 2, respectively. Specimens are characterized by low total REE concentrations, ranging from 14 to 29 ppm in whole rock analyses. The total REE content of individual minerals tends to be higher for dolomite (9–78 ppm) than for magnesite (14–17 ppm; Table 3). Normalized to chondritic REE abundances, both whole-rock and mineral data show enrichment in light REE relative to heavy REE (Table 3). The chondrite-normalized REE patterns for whole-rock analyses and those from individual minerals (magnesite, dolomite and chlorite) show similar convex-upward patterns that have peak abundances at Sm and Eu (Fig. 6). In this respect, the REE patterns for whole-rock samples from Quartz Creek (Fig. 6A) contrast with the REE pattern for the North American Shale Composite, which is relatively enriched in light and heavy REE and depleted in the middle REE.

The shapes of average dolomite, magnesite and chlorite REE patterns are similar (Fig. 6B). The data in Table 3 and Figure 6 do not reveal any significant positive or negative anomalies for Ce or Eu. Magnesite analyses indicate a small positive Eu anomaly (Eu/Eu*) but there is no consistent pattern for Ce/Ce* values (Table 3). This is interesting because prominent Ce or Eu anomalies are commonly seen in carbonate rocks and have been used to infer the origins of some magnesite deposits (e.g. Bau and Möller 1992).

Titanite Dating

U–Pb Titanite dating was performed on sample PIN 4, using 24 spot analyses distributed across 17 individual grains; results for unknowns and standards are listed in Table 4. The analyzed titanite grains showed consistent textural features suggesting that they represent a single generation, and all are associated with magnesite. The analyses show varying degrees of common Pb incorporation in Tera-Wasserburg concordia space (Table 4; Fig. 7A). A subset of 18 analyses defines an isochron with a $^{238}U/^{206}Pb$ intercept of 433 ± 12 Ma (2SE; s = 0.63) with a $^{207}Pb/^{206}Pb$ intercept of 0.83 using the robust regression method of Powell et al. (2020). The isochron age overlaps with a ^{207}Pb-corrected $^{206}Pb/^{238}U$ weighted mean age (following Stacey and Kramers 1975) defined by 11 of the 24 analyses. This second method indicates a slightly older age of 442 ± 10 (MSWD = 3.6), shown in Figure 7B. The overlapping ages indicate that titanite formed in Late Ordovician–Early Silurian times. In the discussion that follows, we suggest that this age also represents the timing of metasomatism that resulted in the formation of pinolite textures.

DISCUSSION

Texture and Mineralogy

Pinolitic textures, such as those observed in magnesite deposits in Austria and Spain, have been interpreted as replacement features produced by Mg-rich hydrothermal fluids

Table 3. Rare earth element ratios and total REE for whole rock analyses and mineral analyses by LA-ICP-MS.

Specimen	Ce/Ce*	Eu/Eu*	Total REE	Total LREE	Total HREE	LREE/ HREE(N)
PIN 1	1.15	1.09	23.26	18.02	5.24	6.48
PIN 2	1.21	0.87	29.09	17.3	11.79	2.33
PIN 3	0.99	1.17	14.34	11.57	2.77	4.67
PIN 4	1.17	0.97	23.59	16.26	7.33	2.76
PIN 5	1.03	1.16	20.82	17.14	3.68	5.91
M-1	0.51	1.74	17	11.3	5.7	0.93
M-2	0.96	1.52	14.32	11.17	3.15	8.15
M-3	1.03	1.55	15.78	12.57	3.21	6.05
D-1	0.95	1.19	78.48	56.9	21.58	3.2
D-2	1.05	1.04	69.51	52.09	17.42	5.28
D-3	1.09	0.99	9.32	6.56	2.76	4.69

Notes: Total REE in ppm. LREE = Light REE (La-Sm). HREE = Heavy REE (Eu-Lu).
Eu/Eu* calculated after Tostevin et al. (2016) normalized to chondrite.
Ce/Ce* calculated after Lawrence et al. (2006) normalized to chondrite.
LREE/HREE(N) calculated as (La + Pr + Nd) / (Er + Tm + Yb + Lu), normalized to chondrite.
Magnesite and dolomite analyses from PIN 3.

(Simandl and Hancock 1991; Lugli et al. 2000; Azim Zadeh et al. 2015). The pinolitic textures at Quartz Creek locally show magnesite crystals with forms indicating growth in opposite directions (termed 'bipolar' textures in some literature) across relict fractures (Fig. 2), and the presence of broken crystals suggests that fracture development and crystal growth were closely linked in time. These and other textures shown in Figure 2 are remarkably similar to those described by Pohl and Siegl (1986; their photos 4, 5 and 8; p. 228, 229 and 231, respectively) from the Austrian and Spanish magnesite deposits. The evidence for multiple fracturing and associated growth episodes (Fig. 2A, 2G) is consistent with crystals formed from the migration of metasomatizing fluids along fractures and bedding surfaces.

There may be two or more generations of dolomite at Quartz Creek. Anhedral, irregularly-shaped dolomite microinclusions within magnesite (Fig. 3B) are consistent with dolomite as a precursor to magnesite formation. The microinclusions are interpreted as relict grains that result from incomplete dolomite replacement. Idiomorphic dolomite grains (Fig. 3A) probably formed later but it is not clear if they are earlier than, later than or contemporaneous with the enclosing magnesite. The relative time of formation or recrystallization of polygrain masses of anhedral dolomite (Fig. 3C) is also unclear and our dolomite analyses do not resolve different populations of dolomite.

Textural observations at some magnesite deposits in British Columbia have suggested a sedimentary and/or early diagenetic origin for magnesite followed by diagenetic or metasomatic replacement to form textures such as pinolite and sparry dolomite (Simandl and Hancock 1991, 1999; Marshall et al. 2004; Paradis and Simandl 2018). The textures from the Quartz Creek area may be similarly related to late hydrothermal replacement of dolomite, as suggested for the Mount Brussilof deposit (Marshall et al. 2004). Although the Quartz

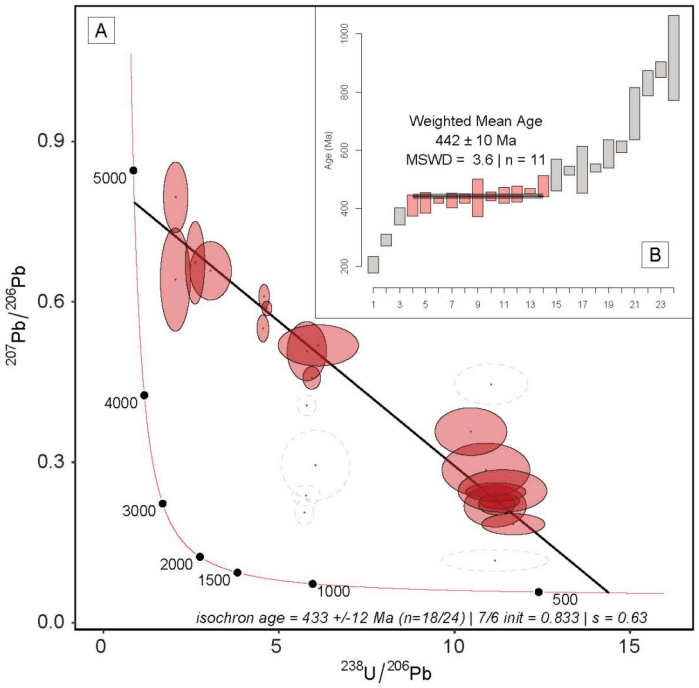

Figure 7. A) Tera-Wasserburg concordia diagram of *in situ* titanite analyses from specimen PIN 4. Red ellipses indicate data included in the calculated isochron age of ca. 433 Ma; unfilled grey dashed ellipses indicate data that were not included. B) a plot of ^{207}Pb-corrected ^{206}Pb/^{238}U ages, in which 11 of 24 determinations define a plateau from which a weighted mean age of ca. 442 Ma is calculated as shown.

Creek rocks and other deposits in British Columbia tend to be associated with dolomitized carbonate host rocks, the possibility of an early diagenetic origin for magnesite from calcite/aragonite limestones is supported by the experiments of Hobbs and Xu (2020). They argue that Veitsch-type magnesite is associated with evaporative environments and their experiments show that it might have formed from calcite through temperature (≤ 40°C) and pH cycling characteristic of evaporative/lagoon/playa environments.

The replacement of dolomite by magnesite proceeds through the following reaction:

$CaMg(CO_3)_2 + 2H+ \rightarrow MgCO_3 + Ca^{2+} + H_2CO_3$ (Aharon 1988; Lugli et al. 2000)

This reaction releases Ca^{2+}, which if accumulated in substantial amounts could reverse the reaction in favour of dolomite. Therefore, calcium must be flushed out by fluids in order for large quantities of magnesite to form (Lugli et al. 2000). This may help to explain textures indicative of dolomite recrystallization (Fig. 3A). Extensive recrystallization of dolomite is a common characteristic of magnesite deposits considered to have formed via metasomatic replacement processes (Aharon 1988; Lugli et al. 2000; Kilias et al. 2006).

The pinolite rocks at Quartz Creek appear to have formed by processes similar to those that generated sparry magnesite deposits in southeastern British Columbia and elsewhere. Other minerals identified in the Quartz Creek specimens, such as quartz and muscovite, along with accessory rutile, pyrite,

Table 4. Geochronology and U–Pb isotopic data for Quartz Creek pinolite titanite. See text for discussion.

Analysis	Approx. U ppm	U/Th	$^{238}U/^{206}Pb$	2SE† %	$^{207}Pb/^{206}Pb$	2SE %	$^{207}Pb/^{235}U$	2SE %	$^{206}Pb/^{238}U$	2SE %	rho
T1-1 C1	58	0.80	11.2	11.2	0.116	14.1	1.44	18	0.0897	11.2	0.62
T1-2 C1	7	0.34	11.2	6.5	0.218	14.7	2.69	16.1	0.0896	6.5	0.40
T1-3 C1	26	0.71	11.2	3.8	0.222	7.4	2.73	8.3	0.0893	3.8	0.46
T1-4 C1	48	0.57	11.7	6.3	0.184	8.8	2.17	10.8	0.0856	6.3	0.58
T2-1 C2	16	0.31	4.54	3.0	0.550	3.8	16.7	4.9	0.2201	3.0	0.62
T3-1 C2	1	0.17	2.05	17.1	0.642	12.3	43.2	21.1	0.4885	17.1	0.81
T4-1 C2	113	1.20	11.3	4.1	0.227	5.2	2.77	6.6	0.0886	4.1	0.62
T4-2 C2	18	0.44	5.94	3.5	0.458	3.8	10.6	5.2	0.1685	3.5	0.68
T5-1 C3	56	0.75	4.58	2.7	0.610	3.0	18.4	4.0	0.2186	2.7	0.67
T5-2 C3	53	0.77	4.66	2.5	0.588	1.9	17.4	3.2	0.2147	2.5	0.80
T6-1 C3	2	1.30	2.06	13.9	0.796	6.8	53.3	15.5	0.4860	13.9	0.90
T7-1 C4	4	0.25	5.80	7.9	0.508	8.9	12.1	11.9	0.1726	7.9	0.66
T8-1 C5	10	0.26	5.79	3.7	0.407	3.9	9.68	5.4	0.1727	3.7	0.68
T9-1 C5	7	0.23	10.9	9.4	0.285	14.5	3.61	17.3	0.0918	9.4	0.54
T10-1 C6	17	0.14	5.73	3.7	0.206	9.5	4.96	10.2	0.1746	3.7	0.36
T10-2 C6	13	0.19	5.77	5.7	0.238	6.4	5.68	8.6	0.1733	5.7	0.67
T10-3 C6	11	0.20	6.04	13.2	0.294	18.1	6.71	22.5	0.1655	13.2	0.59
T11-1 C7	18	0.42	6.12	15.3	0.519	6.1	11.7	16.5	0.1634	15.3	0.93
T11-2 C7	9	0.35	10.5	8.0	0.357	10.2	4.70	13.0	0.0955	8.0	0.62
T11-3 C7	141	0.66	11.2	6.3	0.244	5.8	3.01	8.5	0.0895	6.3	0.73
T11-4 C7	938	2.30	11.4	9.1	0.246	13.2	2.99	16.0	0.0880	9.1	0.57
T12-1 C8	5	0.15	3.06	15.8	0.658	6.8	29.7	17.2	0.3274	15.8	0.92
T13-1 C9	3	0.32	2.61	8.6	0.673	9.4	35.5	12.7	0.3830	8.6	0.68
T14-1 C9	11	0.56	11.0	7.7	0.446	7.0	5.56	10.4	0.0906	7.7	0.74

Table 4. *(continued)* Geochronology and U–Pb isotopic data for Quartz Creek pinolite titanite. See text for discussion.

Analysis	$^{207}Pb/^{206}Pb$ Date (Ma)	2SE ABS	$^{207}Pb/^{235}U$ Date (Ma)	2SE ABS	$^{206}Pb/^{238}U$ Date (Ma)	2SE ABS	$^{206}Pb/^{238}U^{*}$ Date (Ma)	2SE ABS
T1-1 C1	1900	530	904	230	554	64	515	61
T1-2 C1	2970	490	1330	370	553	38	446	38
T1-3 C1	2990	240	1340	210	551	22	442	21
T1-4 C1	2690	290	1170	210	530	35	449	31
T2-1 C2	4380	110	2920	610	1280	43	539	40
T3-1 C2	4600	360	3850	2300	2560	520	916	330
T4-1 C2	3030	170	1350	170	547	23	435	20
T4-2 C2	4110	110	2490	450	1000	38	530	30
T5-1 C3	4530	86	3010	560	1270	37	428	34
T5-2 C3	4480	56	2960	450	1250	35	460	23
T6-1 C3	4910	200	4060	2300	2550	420	206	210
T7-1 C4	4260	270	2610	900	1030	87	476	73
T8-1 C5	3930	120	2400	420	1030	41	612	32
T9-1 C5	3390	470	1550	490	566	55	410	50
T10-1 C6	2870	310	1810	410	1040	41	877	44
T10-2 C6	3100	200	1930	400	1030	64	831	55
T10-3 C6	3440	590	2070	930	987	140	725	120
T11-1 C7	4290	180	2580	1100	976	160	436	80
T11-2 C7	3740	320	1770	480	588	49	373	41
T11-3 C7	3150	190	1410	230	552	36	428	29
T11-4 C7	3160	430	1400	400	544	51	419	45
T12-1 C8	4640	200	3480	1800	1830	320	533	140
T13-1 C9	4670	270	3650	1700	2090	210	587	190
T14-1 C9	4070	210	1910	460	559	45	291	32

*^{207}Pb-corrected following the method of Stacey and Kramers 1975
†2SE = 2 standard error
Standards MMc and Fish gave weighted mean average ages of 528 ± 5 Ma (n=8; MSWD=0.65) and 27.9 ± 1 Ma (n=8; MSWD=0.99), respectively; for other details, see analytical methods.

apatite and zircon, are common relict minerals in many magnesite deposits interpreted to have formed from Mg-rich hydrothermal fluids (Kilias et al. 2006; Azim Zadeh et al. 2015). A fluid inclusion study of the Mount Brussilof deposit indicated temperatures between ~ 200 and 300°C at pressures < 2.6 Kbar (Marshall et al. 2004). Thus, sparry magnesite is apparently of hydrothermal origin but the dark matrix in the Quartz Creek pinolite probably represents relict wall rock as it contains carbonaceous material (graphite?) and zircon grains interpreted to be of detrital origin. The classification of zircon as detrital is based on large variations in the size and shape of zircon grains, and also on the proportions and types of inclusions (Fig. 3). Pyrite may also be detrital but could have formed from reducing hydrothermal fluids (Prochaska 2016). In summary, the sparry magnesite textures appear to reflect metasomatic transformation of dolomite by Mg-rich hydrothermal fluids, and the black matrix represents relict material from the original sedimentary rocks, including some accessory mineral populations.

Whole Rock and Mineral Compositions

Negative correlations of CaO and Sr with MgO and positive correlations between Fe_2O_3 and MgO in whole-rock analyses (Fig. 4) largely reflect the composition and varying proportions of magnesite, dolomite, and chlorite within the samples although there may be some influence from the closed-sum nature of these data. Given the small number of samples, it is difficult to draw further conclusions.

Because dolomite abundances control whole-rock Ca concentrations, and Sr^{2+} substitutes for Ca^{2+} in dolomite, the low and high Sr content in PIN 4 and PIN 5 likely reflects contrasting proportions of dolomite in each sample. FeO varies from 1.4 to 2.5 wt. % in mineral analyses of magnesite and chlorite (Table 2), where Fe^{2+} substitutes for Mg^{2+}. The modal abundances of magnesite are typically higher than those of chlorite, so it is likely that magnesite controls whole-rock Fe_2O_3 concentration in sparry magnesite rocks (Möller 1989). Whole rock Fe_2O_3 varies from 0.77 to 1.96 wt. % (Table 1; average 1.19) and these concentrations largely overlap those for other magnesite-bearing rocks from southeastern British Columbia discussed by Simandl (2002).

Whole-rock SiO_2 contents are controlled by the abundance of chlorite and quartz and the high SiO_2 concentrations in PIN 2 (Table 1) reflect the presence of a quartz vein. Magnesite and dolomite mineral analyses contain negligible Al_2O_3 (Table 2) so whole-rock Al_2O_3 concentrations (Table 1) may reflect the abundances of chlorite and minor clay minerals. The low contents of CaO (up to 0.86 wt. %; Table 2) in Quartz Creek magnesite likely reflect microinclusions of dolomite identified via petrographic studies. Azim Zadeh et al. (2015) attributed elevated CaO (up to 1.32 wt. %) in EMPA analyses of magnesite from the Hohentauern/Sunk sparry magnesite deposit to microinclusions of dolomite and/or redolomitization.

Comparisons with Other Pinolite and Magnesite Deposits

Magnesite and dolomite compositions from Quartz Creek and other sediment-hosted, metasomatic magnesite deposits hosting pinolite-textured rocks (Eugui and Rubian, Spain; Hohentauern/Sunk, Austria) are compared in Table 5 (data from Lugli et al. 2000; Kilias et al. 2006; Azim Zadeh et al. 2015). Mean contents of MgO in magnesite and MgO and CaO in dolomite at Quartz Creek tend to be slightly higher than for the same minerals in these magnesite deposits, but the FeO contents are similar (Table 5). Schroll (2002) determined that magnesite associated with ultramafic rocks contains up to 5 wt. % FeO, compared to only 1–2% FeO for magnesite derived from a sedimentary protolith (Table 5). The low FeO contents of magnesite from Quartz Creek and other deposits confirm that they are likely of sedimentary origin, consistent with the nature of their host rocks.

Trace Element Composition

Trace element (Cr, Ni, Co, Fe, Mn, Ba, Sr) concentrations in magnesite can distinguish types of magnesite deposits (Möller 1989; Azim Zadeh 2009) and have been used to discriminate the sources of Mg^{2+}. Figure 8 compares the concentrations of most of these elements in Quartz Creek magnesite to the mode and median values for magnesite reported by Azim Zadeh (2009; see Fig. 8 caption for details). Magnesite that is associated with ultramafic host rocks is typically enriched in Cr, Ni, and Co, but lower concentrations of these elements suggest formation by sedimentary processes or metasomatism (Azim Zadeh 2009; Kuşcu et al. 2017). Magnesite from Quartz Creek shows very low concentrations of Cr, Ni, and Co and some values are below detection limits. Compared to magnesite from most environments, Ba and Sr are low in Quartz Creek magnesite (Fig. 8). Low Sr and Ba concentrations in magnesite are consistent with its formation in a metasomatic environment because dissolution of primary/diagenetic dolomite releases significant amounts of Ca as well as Sr and Ba into fluids, and these elements are unlikely to replace Mg^{2+} in magnesite (Möller 1989; Azim Zadeh 2009).

Rare Earth Elements

The REE are useful indicators of fluid composition and the physio-chemical environment of mineral formation and can be used to identify the origins of carbonate rocks and minerals (Kiesl et al. 1990; Bau and Möller 1992). Rare earth element enrichment in carbonate minerals can occur by interaction with pore waters, from which REE are typically incorporated into the carbonate crystal lattice by substituting for Ca^{2+} and Mg^{2+}. They can also occupy lattice positions which are free due to structural defects and in some cases form separate REE carbonate minerals (Qing and Mountjoy 1994; Bau and Alexander 2006). Whole-rock (carbonate) REE signatures can be overprinted by interaction with fluids and can be difficult to interpret due to the presence of other minerals such as Fe-oxides, clay minerals, quartz and sulphides (Frimmel 2009; Zhang et al. 2014). The whole-rock REE patterns displayed by the Quartz Creek pinolite rocks differ significantly from the North America Shale Composite pattern and have convex-upward shapes with a modest peak at Sm and Eu (Fig. 6A). Previous studies on the formation of dolomite attributed high Sm_N/Yb_N to

Table 5. Mean MgO, CaO and FeO composition of dolomite and magnesite from Quartz Creek and other sparry magnesite deposits.

Deposit		Magnesite			Dolomite		
		MgO	CaO	FeO	MgO	CaO	FeO
Quartz Creek, Canada	Mean	49.38	0.56	1.80	24.88	33.33	0.53
	SD	1.04	0.40	0.62	0.68	0.60	0.05
	n	3	3	3	3	3	3
Rubian, Spain	Mean	47.8	0.41	1.16	22.7	26.6	0.42
	SD	1.4	0.25	0.63	1.8	1.6	0.11
	n	36	36	36	11	11	11
Eugui, Spain	Mean	45.8	0.41	1.82	21.3	30.2	1.04
	SD	1.4	0.26	1.91	1.6	0.5	1.1
	n	78	78	78	77	77	77
Hohentauern/Sunk, Austria	Mean	47.0	0.42	2.0	21.7	29.0	1.48
	SD	0.9	0.42	0.5	1.6	2.9	0.74
	n	17	17	17	6	6	6

Notes: Concentrations in oxide wt.%. SD = standard deviation and n = number of analyses.
Data from Table 2 and Lugli et al. 2000; Kilias et al. 2006; Azim Zadeh et al. 2015.

reducing Fe oxides in pore waters which preferentially take up REE in the middle part of the sequence (Sm to Gd) and release them into carbonates under reducing conditions (Haley et al. 2004; Huang et al. 2009; Navarro-Ciurana et al. 2017; Callen and Herrmann 2019). This suggests that the sedimentary dolomite precursor may have formed under reducing conditions and that later-formed magnesite and chlorite inherited its geochemical signature. The lack of characteristic seawater REE patterns and the similarity between REE profiles of each sample (Fig. 6A) and its constituent minerals (Fig. 6B) suggests that the original rocks reacted with fluids that did not have seawater geochemical signatures.

Evaporite magnesite typically shows very low REE contents. This reflects early removal of the REE from seawater as Ca-rich minerals precipitate prior to magnesite saturation (Möller 1989). Magnesite analyses from Quartz Creek samples have higher REE contents than seawater and thus are unlikely to represent evaporitic magnesite. Seawater-derived carbonate rocks typically exhibit depletion of light REE depletion relative to heavy REE, which is the exact opposite of the pattern show by whole-rock and mineral data from the Quartz Creek samples. The Quartz Creek whole-rock REE trends (Fig. 6A) are more consistent with precipitation from hydrothermal fluids that did not have seawater geochemical signatures (Callen and Herrmann 2019). Magnesite that precipitates directly from hydrothermal fluids tends to be depleted in light REE-because the heavy REE are more easily accepted into the magnesite crystal lattice (Möller 1989; Bau and Möller 1992; Lugli et al. 2000). In contrast, Quartz Creek magnesite displays an overall relative enrichment in the light REE (Fig. 6B).

Europium and/or Ce anomalies are common in carbonates and can be indicative of high-temperature hydrothermal fluids or reducing or oxidizing conditions in aqueous systems (Bau and Möller 1992). Normal seawater-derived carbonate rocks typically display negative Ce anomalies. These features are not present in the whole-rock REE profiles from the Quartz Creek samples, or in REE profiles for individual minerals at Quartz Creek (Fig. 6). The oxidation state of europium (Eu^{3+}/Eu^{2+}) is primarily controlled by temperature, and positive Eu anomalies can be indicative of high-temperature hydrothermal fluids (Frimmel 2009; Meyer et al. 2012; Tostevin et al. 2016). Calculated Eu anomalies (Eu/Eu*) for Quartz Creek magnesite are only weakly positive, but the negative Eu anomalies associated with sedimentary environments are not observed.

Age and Tectonic Implications

Powell et al. (2006) suggested that the magnesite deposits of southeastern British Columbia formed through the influence of Mg-rich brines mobilized by heat and faulting during Cambrian rifting and subsidence. The only stratigraphic constraint on when the pinolite textures at Quartz Creek formed is that they must either be of the same age or younger than their Neoproterozoic host rocks. The stratigraphic ages of sedimentary rocks hosting sparry magnesite deposits in southern British Columbia range from as young as Middle Cambrian (Mount Brussilof; Fritz and Simandl 1993; Marshall et al. 2004) to as old as Mesoproterozoic (Brisco and Driftwood Creek; Simandl and Hancock 1992).

Our Late Ordovician to Early Silurian titanite U–Pb age (433 ± 12 Ma) from Quartz Creek is based on isotopic analyses of many titanite grains, with no obvious textural differences, that are closely associated with pinolitic magnesite crystals and magnesite in micro-veins. We suggest that it provides a reliable estimate for the timing of formation of the pinolite textures, and it indicates that these are much younger than the Neoproterozoic depositional age of the Horsethief Creek Group host rocks. The Tera-Wasserburg concordia plot is interpreted to define a regression line caused by variable amounts of alteration of individual grains, which intersects the concordia curve at ~ 433 Ma. This is consistent with the 442 Ma age implied by the weighted average of $^{238}U/^{206}Pb$ ages (Fig. 7).

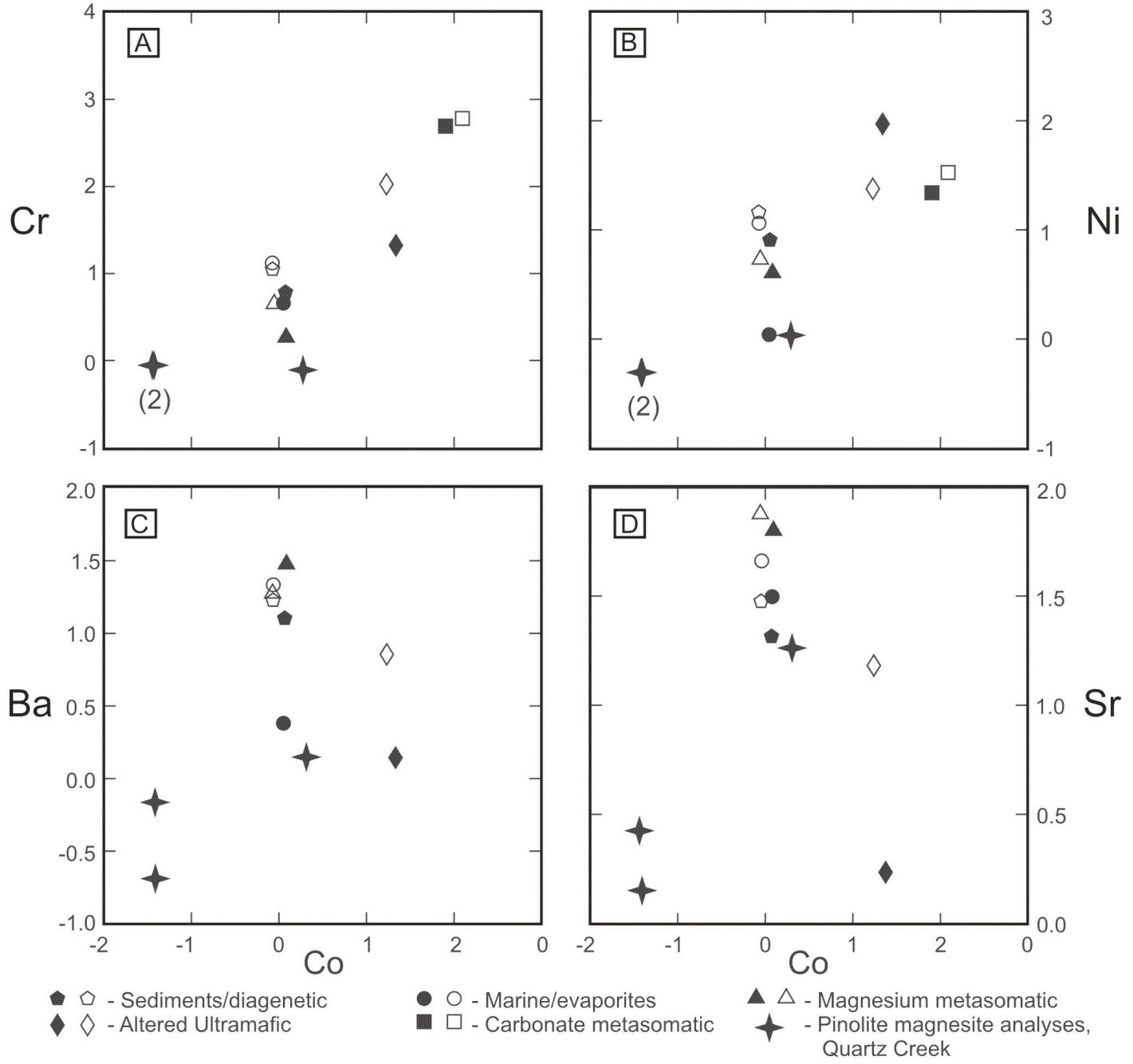

Figure 8. Log_{10} Co versus Log_{10} Ni, Cr, Ba and Sr plots comparing magnesite from the Quartz Creek pinolite rocks with the reported concentrations of these elements in magnesite from various environments. The Quartz Creek magnesite most closely resembles magnesite interpreted to be formed through metasomatic processes. It is also similar to evaporitic/marine magnesite but is distinctly different from magnesite in altered ultramafic and CO_2 metasomatic environments. The comparative data were extracted from element concentration-frequency graphs in Azim Zadeh (2009) that summarized data from Möller (1989). They reflect the most likely concentrations of elements in each environment while de-emphasizing outliers. Note that all Cr analyses and two Ni analyses from Quartz Creek were below the detection limit so comparisons for these elements may be unreliable.

The Late Ordovician to Early Silurian age suggested for the Quartz Creek pinolite locality is consistent with aspects of the regional geology. Cambrian to Late Ordovician mafic volcanic rocks and lithologically similar diatremes occur in a narrow, SE trending, 160 km-long belt that extends through Golden, BC (Pell 1986; Larson and Price 2006). Emplacement of these igneous rocks appears to have been controlled by basement faults defining the margin between the Paleozoic miogeocline to the west and the Laurentian craton to the east (Larson and Price 2006). The faulting, igneous activity and heat associated with these Cambrian to Ordovician tectonic events may have provided conduits, sources, and thermal energy for migrating hydrothermal fluids that formed the pinolite textures at Quartz Creek and perhaps other locations in southeastern British Columbia.

CONCLUSIONS

Distinctive and unusual pinolitic textures developed in carbonate rocks of the Neoproterozoic Horsethief Creek Group near Golden, British Columbia, are interpreted to have formed by metasomatic processes that led to the replacement of primary dolomite by magnesite, in response to the effects of Mg-rich hydrothermal fluids. Textural observations such as broken crystals, and multiple fracturing and growth episodes, support a model where metasomatic fluids moved along fractures and bedding surfaces. Petrographic observations of dolomite microinclusions within magnesite and evidence for recrystallization of dolomite are also consistent with metasomatic replacement. A Late Ordovician to Early Silurian U–Pb age for titanite grains that are intimately associated with magnesite indicates that the development of pinolitic textures occurred long after deposition of the Neoproterozoic host rocks of the Horsethief Creek Group. This age is also younger than the Middle Cambrian sedimentary rocks that host the Mount Brussilof magnesite deposit (Fritz and Simandl 1993; Marshall et al. 2004) and the Mesoproterozoic sedimentary rocks that host the Brisco and Driftwood Creek deposits (Simandl and Hancock 1992). The U–Pb titanite age from Quartz Creek is broadly coeval with fault-related diatremes and volcaniclastic rocks that may also have supplied heat and/or fluids for metasomatic processes.

Geochemical investigations of the Quartz Creek pinolite occurrence are hampered by the small number of analyzed samples, but preliminary data suggest that whole-rock and mineral compositions resemble those of other magnesite deposits that contain pinolitic textures, which have similarly been interpreted to result from metasomatic processes. In particular, REE profiles for samples and minerals from Quartz Creek lack the distinctive Ce and Eu anomalies that are associated with seawater, and REE concentrations are higher than those documented from magnesite of primary evaporitic origin. The similarity of REE profiles for individual minerals such as dolomite and magnesite, and the enrichment of light REE relative to heavy REE, are also consistent with an influence from hydrothermal fluids. It is suggested that systematic geochemical studies of other magnesite deposits, and efforts to obtain their formation ages through dating accessory minerals associated with pinolite, might prove useful avenues for future research on this and related topics.

ACKNOWLEDGEMENTS

Ian Burak and Canadian Pinolite Corporation provided samples and contributed to analytical expenses. D. Wilson took the sculpture photograph. The Department of Earth, Environmental and Geographic Sciences at UBC Okanagan also helped with analytical expenses. Larson acknowledges support from a NSERC Discovery Grant. Polished thin sections were prepared by S. Wood. The Fipke Laboratory for Trace Element Research (FiLTER) and technicians S. Shrestha and M. Button made possible mineral trace element and isotopic analyses. L. Ersay provided advice. R. Corney drafted two diagrams. Comments by an anonymous journal reviewer and J. Conliffe led to substantial improvements to the manuscript. Editor A. Kerr and copy editor S. Amor suggested wording improvements and modifications. Brian Pratt is thanked for his input as the section editor for the series.

REFERENCES

Aharon, P., 1988, A stable-isotope study of magnesites from the Rum Jungle uranium field, Australia: implications for the origin of strata-bound massive magnesites: Chemical Geology, v. 69, p. 127–145, https://doi.org/10.1016/0009-2541(88)90164-7.

Azim Zadeh, A.M., 2009, The genetic model of the Hohentauern/Sunk sparry magnesite deposit (Eastern Alps/Austria): Unpublished PhD thesis, University of Leoben, Leoben, Austria, 182 p.

Azim Zadeh, A.M., Ebner, F., and Jiang, S.-Y., 2015, Mineralogical, geochemical, fluid inclusion and isotope study of Hohentauern/Sunk sparry magnesite deposit (Eastern Alps/Austria): implications for a metasomatic genetic model: Mineralogy and Petrology, v. 109, p. 555–575, https://doi.org/10.1007/s00710-015-0386-2.

Bau, M., and Alexander, B., 2006, Preservation of primary REE patterns without Ce anomaly during dolomitization of Mid-Paleoproterozoic limestone and the potential re-establishment of marine anoxia immediately after the "Great Oxidation Event": South African Journal of Geology, v. 109, p. 81–86, https://doi.org/10.2113/gssajg.109.1-2.81.

Bau, M., and Möller, P., 1992, Rare earth element fractionation in metamorphogenic hydrothermal calcite, magnesite and siderite: Mineralogy and Petrology, v. 45, p. 231–246, https://doi.org/10.1007/BF01163114.

Callen, J.M., and Herrmann, A.D., 2019, In situ geochemistry of middle Ordovician dolomites of the upper Mississippi valley: The Depositional Record, v. 5, p. 4–22, https://doi.org/10.1002/dep2.51.

Frimmel, H.E., 2009, Trace element distribution in Neoproterozoic carbonates as palaeoenvironmental indicator: Chemical Geology, v. 258, p. 338–353, https://doi.org/10.1016/j.chemgeo.2008.10.033.

Fritz, W.H., and Simandl, G.J., 1993, New middle Cambrian fossil and geological data from the Brussilof magnesite mine area, southeastern British Columbia: Geological Survey of Canada, Paper 93-1A, p. 183–190, https://doi.org/10.4095/134205.

Gromet, L.P., Haskin, L.A., Korotev, R.L., and Dymek, R.F., 1984, The "North American shale composite": Its compilation, major and trace element characteristics: Geochimica et Cosmochimica Acta, v. 48, p. 2469–2482, https://doi.org/10.1016/0016-7037(84)90298-9.

Haley, B.A., Klinkhammer, G.P., and McManus, J., 2004, Rare earth elements in pore waters of marine sediments: Geochimica et Cosmochimica Acta, v. 68, p. 1265–1279, https://doi.org/10.1016/j.gca.2003.09.012.

Hancock, K.D., and Simandl, G.J., 1992, Geology of the Marysville Magnesite Deposit, Southeastern British Columbia: British Columbia Ministry of Energy, Mines and Petroleum Resources, Exploration in British Columbia, Part B, p. 71–80.

Hobbs, F.W.C., and Xu, H., 2020, Magnesite formation through temperature and pH cycling as a proxy for lagoon and playa paleoenvironments: Geochimica et Cosmochimica Acta, v. 269, p. 101–116, https://doi.org/10.1016/j.gca.2019.10.014.

Huang, J., Chu, X.L., Chang, H.J., and Feng, L.J., 2009, Trace element and rare earth element of cap carbonate in Ediacaran Doushantuo Formation in Yangtze Gorges: Chinese Science Bulletin, v. 54, p. 3295–3302, https://doi.org/10.1007/s11434-009-0305-1.

Kiesl, W., Koeberl, C., and Körner, W., 1990, Geochemistry of magnesites and dolomites at the Oberdorf/Laming (Austria) deposit and implications for their origin: Geologische Rundschau, v. 79, p. 327–335, https://doi.org/10.1007/BF01830629.

Kilias, S.P., Pozo, M., Bustillo, M., Stamatakis, M.G., and Calvo, J.P., 2006, Origin of the Rubian carbonate-hosted magnesite deposit, Galicia, NW Spain: mineralogical, REE, fluid inclusion and isotope evidence: Mineralium Deposita, v. 41, p. 713–733, https://doi.org/10.1007/s00126-006-0075-5.

Krupenin, M.T., 2005, Geological-geochemical types and REE systematization in deposits of the South Urals magnesite province: Doklady Earth Sciences, v. 405, p. 1253–1256.

Krupenin, M.T., and Ellmies, R., 2001, Genetic features of sparry magnesites in Proterozoic carbonate rocks of the Southern Urals: Ethnographic Praxis in Industry Conference Proceedings, v. 6, p. 997–999.

Kubli, T.E., 1990, Geology of the Dogtooth Range, Northern Purcell Mountains, British Columbia: Unpublished PhD thesis, University of Calgary, Calgary, Canada, 324 p. https://doi.org/10.11575/PRISM/19577.

Kuşcu, M., Cengiz, O., and Kahya, A., 2017, Trace element contents and C-O isotope geochemistry of the different originated magnesite deposits in Lake District (Southwestern Anatolia), Turkey: Arabian Journal of Geosciences, v. 10, 339, https://doi.org/10.1007/s12517-017-3102-1.

Larson, K.P., and Price, R.A., 2006, The southern termination of the Western Main Ranges of the Canadian Rockies, near Fort Steele, British Columbia: stratigraphy, structure, and tectonic implications: Bulletin of Canadian Petroleum Geology, v. 54, p. 37–61, https://doi.org/10.2113/54.1.37.

Lawrence, M.G., Greig, A., Collerson, K.D., and Kamber, B.S., 2006, Rare earth ele-

ment and Yttrium variability in southeast Queensland Waterways: Aquatic Geochemistry, v. 12, p. 39–72, https://doi.org/10.1007/s10498-005-4471-8.

Lugli, S., Torres-Ruiz, J., Garuti, G., and Olmedo, F., 2000, Petrography and geochemistry of the Eugui magnesite deposit (Western Pyrenees, Spain): Evidence for the development of a peculiar zebra banding by dolomite replacement: Economic Geology, v. 95, p. 1775–1791, https://doi.org/10.2113/95.8.1775.

Marshall, D., Simandl, G., and Voormeij, D., 2004, Fluid inclusion evidence for the genesis of the Mount Brussilof magnesite deposit, *in* Simandl, G.J., McMillan, W.J., and Robinson, N.D., *eds.*, Industrial Minerals with Emphasis on Western North America: British Columbia Ministry of Energy and Mines, Geological Survey Paper 2004–2, p. 65–75.

McDonough, W.F., and Sun, S.-s., 1995, The composition of the Earth: Chemical Geology, v. 120, p. 223–253, https://doi.org/10.1016/0009-2541(94)00140-4.

Meyer, E.E., Quicksall, A.N., Landis, J.D., Link, P.K., and Bostick, B.C., 2012, Trace and rare earth elemental investigation of a Sturtian cap-carbonate, Pocatello, Idaho: Evidence for ocean redox conditions before and during carbonate deposition: Precambrian Research, v. 192–195, p. 89–106, https://doi.org/10.1016/j.precamres.2011.09.015.

Möller, P., 1989, Minor and trace elements in magnesite monograph series on mineral deposits: Gebrüder Borntrager, Berlin-Stutgart, v. 28, p. 173–195.

Navarro-Ciurana, D., Cardellach, E., Galindo, C., Fuenlabrada, J.M., Griera, A., Gómez-Gras, D., Vindel, E., and Corbella, M., 2017, REE and Sm–Nd clues of high temperature fluid rock interaction in the Riópar dolomitization (SE Spain): Procedia Earth and Planetary Science, v. 17, p. 448–451, https://doi.org/10.1016/j.proeps.2016.12.113.

Nesbitt, B. E., and Prochaska, W., 1998, Solute chemistry of inclusion fluids from sparry dolomites and magnesites in Middle Cambrian carbonate rocks of the southern Canadian Rocky Mountains: Canadian Journal of Earth Sciences, v. 35, p. 546–555, https://doi.org/10.1139/e98-006.

Paradis, S., and Simandl, G.J., 2018, Are there genetic links between carbonate-hosted barite-zinc-lead sulphide deposits and magnesite mineralization in southeast British Columbia?, *in* Rogers, N., *ed.,* Targeted Geoscience Initiative: 2017 Report of Activities, Volume 1, Geological Survey of Canada Open File 8358, p. 217–227, https://doi.org/10.4095/306478.

Pearce, N.J.G., Perkins, W.T., Westgate, J.A., Gorton, M.P., Jackson, S.E., Neal, C.R., and Chenery, S.P., 1997, A compilation of new and published major and trace element data for NIST SRM 610 and NIST SRM 612 glass reference materials: Geostandards Newsletter, v. 21, p. 115–144, https://doi.org/10.1111/j.1751-908X.1997.tb00538.x.

Pell, J., 1986, Diatreme breccias in British Columbia: Geological Fieldwork 1985, British Columbia Ministry of Energy, Mines and Petroleum Resources, Paper 1986-1, p. 243–253.

Pohl, W., 1989, Comparative geology of magnesite deposits and occurrences: Monograph Series on Mineral Deposits, v. 28, p. 1–13.

Pohl, W., 1990, Genesis of magnesite deposits - models and trends: Geologische Rundschau, v. 79, p. 291–299, https://doi.org/10.1007/BF01830626.

Pohl, W., 2011, Economic Geology: Principles and Practice: Wiley-Blackwell, 678 p., https://doi.org/10.1002/9781444394870.

Pohl, W., and Siegl, W., 1986, Sediment hosted magnesite deposits, *in* Wolf, K.H., *ed.,* Handbook of Stratabound and Stratiform ore deposits: Elsevier, v. 14, p. 223–260.

Poulton, T.P., 1973, Upper Proterozoic 'Limestone Unit', Northern Dogtooth Mountains, British Columbia: Canadian Journal of Earth Sciences, v. 10, p. 292–305, https://doi.org/10.1139/e73-026.

Poulton, T.P., and Simony, P.S., 1980, Stratigraphy, sedimentology, and regional correlation of the Horsethief Creek Group (Hadrynian, Late Precambrian) in the northern Purcell and Selkirk Mountains, British Columbia: Canadian Journal of Earth Sciences, v. 17, p. 1708–1724, https://doi.org/10.1139/e80-179.

Powell, R., Green, E.C.R., Marillo Sialer, E., and Woodhead, J., 2020, Robust isochron calculation: Geochronology, v. 2, p. 325–342, https://doi.org/10.5194/gchron-2-325-2020.

Powell, W.G., Johnston, P.A., Collom, C.J., and Johnston, K.J., 2006, Middle Cambrian brine seeps on the Kicking Horse Rim and their relationship to talc and magnesite mineralization and associated dolomitization, British Columbia, Canada: Economic Geology, v. 101, p. 431–451, https://doi.org/10.2113/ gsecongeo.101.2.431.

Prochaska, W., 2016, Genetic concepts on the formation of the Austrian magnesite and siderite mineralizations in the Eastern Alps of Austria: Geologia Croatica, v. 69, p. 31–38, https://doi.org/10.4154/GC.2016.03.

Qing, H., and Mountjoy, E.W., 1994, Formation of coarsely crystalline, hydrothermal dolomite reservoirs in the Presqu'ile Barrier, Western Canada Sedimentary Basin: AAPG Bulletin, v. 78, p. 55–77, https://doi.org/10.1306/BDFF9014-1718-11D7-8645000102C1865D.

Redlich, K.A., 1909, Die Typen der Magnesitlagerstätten: Zeitschr. f. prakt. Geologie, v. 17, p. 300–310.

Schroll, E., 2002, Genesis of magnesite deposits in the view of isotope geochemistry: Boletim Paranaense de Geociências, v. 50, p. 59–68, https://doi.org/10.5380/geo.v50i0.4158.

Simandl, G.J., 2002, The chemical characteristics and development potential of magnesite deposits in BC, *in* Scott, P.W., and Bristow, C.M., *eds.*, Industrial Minerals and Extractive Industry Geology: Geological Society of London, p. 169–178.

Simandl, G.J., and Hancock, K.D., 1991, Geology of the Mount Brussilof magnesite deposit, southeastern British Columbia, *in* Geological Fieldwork 1990, British Columbia Ministry of Energy, Mines and Petroleum Resources, Paper 1991-1, p. 269–278.

Simandl, G.J., and Hancock, K.D., 1992, Geology of the Dolomite-hosted Magnesite Deposits of Brisco and Driftwood Creek areas, British Columbia, *in* Geological Fieldwork 1991, British Columbia Ministry of Mines and Petroleum Resources, Paper 1992-1, p. 461–478.

Simandl, G.J., and Hancock, K., 1999, Sparry magnesite, *in* Selected mineral deposit profiles, volume 3 - industrial minerals and gemstones: British Columbia Ministry of Energy and Mines, British Columbia Geological Survey Open File 1999-10, p. 39–41.

Simandl, G.J., Hancock, K.D., Fournier, M.A., Koyanagi, V.M., Vilkos, V., Lett, R.E., and Colbourne, C., 1992, Geology and major element geochemistry of the Mount Brussilof magnesite area, Southeastern British Columbia (082J/ 12, 13): British Columbia Ministry of Energy, Mines and Petroleum Resources, Mineral Resources Division, Geological Survey Branch, Open File 1992-14, p. 1–14 plus map.

Stacey, J.S., and Kramers, J.D., 1975, Approximation of terrestrial lead isotope evolution by a two-stage model: Earth and Planetary Science Letters, v. 26, p. 207–221, https://doi.org/10.1016/0012-821X(75)90088-6.

Tostevin, R., Shields, G.A., Tarbuck, G.M., He, T., Clarkson, M.O., and Wood, R.A., 2016, Effective use of cerium anomalies as a redox proxy in carbonate-dominated marine settings: Chemical Geology, v. 438, p. 146–162, https://doi.org/10.1016/j.chemgeo.2016.06.027.

Wheeler, J.O., and Fox, P.E., 1962, Geology, Rogers Pass, Golden, West Half, British Columbia – Alberta: Geological Survey of Canada Map 43-1962, 1 Sheet, https://doi.org/10.4095/108810.

Zhang, W., Guan, P., Jian, X., Feng, F., and Zou, C., 2014, *In situ* geochemistry of Lower Paleozoic dolomites in the northwestern Tarim basin: Implications for the nature, origin, and evolution of diagenetic fluids: Geochemistry, Geophysics, Geosystems, v. 15, p. 2744–2764, https://doi.org/10.1002/2013GC005194.

Received February 2021
Accepted as revised September 2021

For access to the Littlejohn-Regular et al. (2021) Supplementary Material: *Appendix A: Detailed Analytical Methods*, please visit the GAC's open source GC Data Repository for the Heritage Stone Series: at: https://gac.ca/gc-data-repository/.